Journal of Crystal Growth 691 (2026) 128669

Contents lists available at ScienceDirect

Journal of Crystal Growth

journal homepage: www.elsevier.com/locate/jcrysgro

A study of the mechanism behind crystal lifting: Crystallization pressure of confined $KAl(SO_4)_2{\cdot}12H_2O$ crystals ☆

Anton Tuluk [a], Erik de Ronde [a], Michael Steiger [b], Barbara Lubelli [c], Hugo Meekes [a], Elias Vlieg [a,*]

[a] Radboud University, Institute for Molecules and Materials, Heyendaalseweg 135, 6525 AJ Nijmegen, The Netherlands
[b] Institut für Anorganische und Angewandte Chemie, Universität Hamburg, Martin-Luther-King-Platz 6, 20146 Hamburg, Germany
[c] Faculty of Architecture and the Built Environment, Delft University of Technology, Delft, The Netherlands

ARTICLE INFO

Communicated by V. Fratello

Keywords:
Crystallization pressure
Potash alum
Crystal lifting

ABSTRACT

Salt crystallization pressure is one of the main sources of weathering in porous building materials. In our work we study the origin of this phenomenon using single crystals of $KAl(SO_4)_2{\cdot}12H_2O$ (potassium aluminium sulphate dodecahydrate) as model system. Crystals were grown immersed in a solution of a specific supersaturation ($\sigma = 10 - 80$ %). Evidence of crystallization pressure was the vertical lift of weights on top of the growing crystal, which was measured by in-situ displacement sensors. A clear supersaturation threshold of $\sigma \simeq 30$ % for a 0.5 N weight is required to initiate lifting in our model system. Above this value, the maximum displacement increases nonlinearly with σ and depends on crystal orientation, interfacial wettability, and applied load. Hydrophobic interfaces suppress crystal growth by limiting mass transport, whereas hydrophilic confinement supports continuous growth until the local supersaturation is exhausted. In saturated solutions, on the other hand, a load leads to dissolution. Based on the observations, we propose a mechanism for crystallization pressure for which the growth of the unloaded faces adjacent to the confined face is key. These results refine our understanding of crystallization pressure in confined spaces and can help explain and mitigate salt-induced damage in porous materials.

1. Introduction

Crystallization of salts within porous and granular materials is a well-recognized cause of damage in construction materials, natural stone, and even geologic formations. When salt solutions evaporate or temperature changes induce crystallization in a confined pore network, the growing crystals can exert force on the pore walls. Over time, this crystallization-induced pressure can lead to crack formation, scaling, or disintegration of materials. This damage is often referred to as salt weathering [1–3]. Understanding the fundamental mechanisms of crystallization pressure is therefore crucial for predicting and preventing such damage [4–6].

The ability of growing crystals to generate force has been documented for over a century. A classic early demonstration was provided by Becker and Day in 1905 [7], who observed that a crystal could literally lift a weight. In their experiment, potassium alum crystals growing against a glass plate were able to raise the plate despite the load on it. This famous experiment provided direct evidence that crystallizing salts can exert substantial pressure on their surroundings. Becker and Day further noted that the actual contact area between the crystal and the plate was much smaller than the apparent area, meaning the local pressure at the contact was very high. In the description of this result, the experiments appear to be straightforward and the effect quite large, but in a more detailed report from 1916 by the same authors [8], it becomes clear that the experiments are difficult, and the effect is small. In the same year, Taber [9] performed similar studies with various salts and confirmed an important limitation: if other crystals were growing freely in the solution (i.e. on other surfaces without confinement), the crystal under load ceased to grow against the weight.

The first quantitative relationship between crystallization-induced stress and solution conditions was formulated by Correns and Steinborn [10,11]. Through a series of experiments in the 1920s–1940s with crystals such as potassium alum growing under controlled loads, Correns measured the maximum pressure applied to a crystal at which the

☆ The research is funded by NWO (Dutch research council) under the project 'Mortars with mixed-in inhibitors for mitigating salt damage- MORISAL' (Grant no. 17636).

* Corresponding author.
E-mail address: e.vlieg@science.ru.nl (E. Vlieg).

https://doi.org/10.1016/j.jcrysgro.2026.128669
Received 27 February 2026; Received in revised form 21 April 2026; Accepted 4 May 2026
Available online 12 May 2026

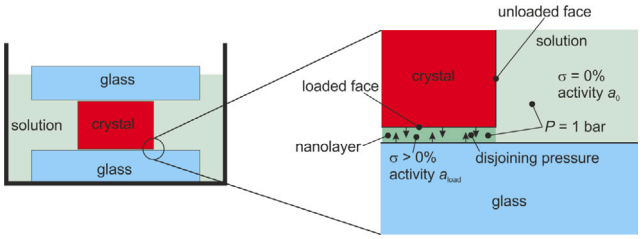

Fig. 1. Schematic of a crystal confined between two surfaces, showing the nanolayer between crystal and substrates (here glass) and the increased solution concentration in this layer as compared to the equilibrium situation in the bulk solution.

crystal could still grow (beyond which growth stopped) and correlated this with the solution's supersaturation. He proposed a thermodynamic expression relating the crystallization pressure to the supersaturation of the salt solution, which became a cornerstone in the field. After Correns' time, research on crystallization pressure was sporadic for several decades. The topic regained significant attention from the late 20-th onwards, when many researchers revisited the problem in the context of material deterioration [12–17]. This showed that Corrrens' thermodynamic expression, though fitting his measured data, was quantitatively in error by roughly a factor of four, mainly due to oversimplified assumptions, such as neglecting ionic activities in solution. The surprising agreement between the experiments and a flawed theory has been extensively discussed [13], but remains somewhat of a mystery. There were likely flaws in the experiments as well, in particular in quantifying the contact area of the interface between the crystal and the support. These are difficult experiments and no one has since reported on the quantitative agreement between crystallization pressure and applied loads.

Steiger [14,18] has provided a review and summary of the thermodynamics of crystallization pressure, and we refer to this work for the theoretical details. Here we summarize the features that are important for understanding the results presented in this paper. Fig. 1 shows a schematic of a crystal in confinement. Crystallization pressure is the pressure Π exerted by a crystal when it grows in a confined space, the confinement leading to stresses at interface of the crystal surface with the surrounding solid surfaces. The stress can be due to the crystal being pressed against a pore wall, the result of a weight on the crystal as in Fig. 1, or even the effect of the crystal's own weight. The load on the crystal will lead to a thin solution layer between the crystal and its support, which we will call nanolayer and is shown enlarged in the right-hand image of Fig. 1. The small spacing between the two solid interfaces, in combination with the interactions within the liquid nanolayer, leads to a repulsive force, which is called the disjoining pressure Π [19]. This is the result of the combined effect of various interactions, including London-van der Waals forces, electrostatic double-layer forces for charged surfaces, and short-range structural (hydration) forces arising from solvent layering near solid interfaces. The forces across the interfaces increase strongly with decreasing distances and become significant in the nanometre range; the liquid film will typically have a thickness in the range of 2–10 nm [17,20]. The nanolayer is only present if the interfacial energies of the surfaces involved do not make a direct solid–solid contact more favourable and if the pressure exerted by the load is less than the maximum disjoining pressure that the interfaces can deliver; at some maximum pressure the nanolayer will collapse. For lifting to occur, a liquid layer has to be present and the disjoining force has to be repulsive.

The crystal in Fig. 1 has faces in two distinct environments: the loaded face is in contact with a solid, while the unloaded one is only in contact with a 'bulk' solution. At equilibrium, the unloaded face is in equilibrium with a saturated solution, i.e. a solution with supersaturation $\sigma = 0$ %. We will call the activity of this solution a_0. The loaded interface, however, has a higher chemical potential, because it experiences a pressure. We emphasize that this pressure is *not* coming from the solution, because this is at the same pressure everywhere (1 bar under normal circumstances). The extra pressure originates from the normal stress corresponding to the disjoining pressure (which counteracts the total force from the weight of the various components). Due to the extra stress, the loaded face is not in equilibrium with a solution with activity a_0, but with a solution with a higher solute activity a_{load}. This corresponds to a positive supersaturation with respect to the bulk solution, and thus in principle diffusion will take place from the nanolayer to the bulk solution, causing growth on the unloaded face and a thinning of the crystal. The system is thus only in a quasi-equilibrium, where the unloaded and loaded interfaces are in local equilibrium with solutions with activities a_0 and a_{load}, respectively.

Steiger has derived the relation between the pressure difference of the loaded and unloaded faces and the corresponding difference in solution activities by considering the chemical potentials of all components involved [14]. The result is:

$$\Pi = \frac{RT}{V_m} \ln \frac{a_{\mathrm{load}}}{a_0}, \tag{1}$$

where R is the gas constant, T the temperature and V_m the molar volume of the crystal. Π is the crystallization pressure, which is, as we have discussed, the same as the disjoining pressure. Calculating the activities of a (super)saturated solution is in general complex [14], but because our experimental values for the pressure have low accuracy, a reasonable estimate of the theoretical values is sufficient here. In Section 2 we show a calculation based on ideal behaviour, and subsequently correct this for non-ideality based on existing literature.

When the bulk solution has activity a_0, no growth occurs and lifting of a weight will not happen. Growth is only possible if the activity in the solution is increased. When the bulk solution is set to an activity with value a, the driving force for crystal growth for the unloaded face is:

$$\Delta\mu = kT \ln \frac{a}{a_0}, \tag{2}$$

with k Boltzmann's constant. Growth will occur for any $a > a_0$. For the loaded face, however, the reference point for the driving force is the activity under load, a_{load}. If the solution activity in the nanolayer is set to a_{layer}, the driving force for crystallization is:

$$\Delta\mu_{\mathrm{load}} = kT \ln \frac{a_{\mathrm{layer}}}{a_{\mathrm{load}}}. \tag{3}$$

At this interface, growth only occurs when $a_{\mathrm{layer}} > a_{\mathrm{load}}$, and thus a_{load} is the threshold value for lifting to occur. For lower values of a_{layer}, the loaded face will (slowly) dissolve. This shows that there is an activity (concentration) range, for which the unloaded face will grow, but the loaded one will not: $a_0 < a < a_{\mathrm{load}}$. The concept of crystallization pressure captures the idea that only for high enough concentrations in the solution, lifting and crystallization damage is possible.

In practice setting the activity in the nanolayer in nearly impossible, because of the limited mass transport. Fig. 1 already showed this: the value in the bulk solution is a_0, but in the nanolayer the local value is a_{load}. The only situation in which the mass transport to or from the nanolayer does not play a role is when the value in the bulk solution is set to a_{load}. Then the solutions in the bulk and in the nanolayer are in equilibrium, and also the loaded face is in equilibrium and will neither grow nor dissolve. In that case there is a positive driving force with respect to the unloaded face, so that face will grow.

Despite significant progress in formulating the concept of crystallization pressure, several knowledge gaps persist. The current literature contains conflicting findings and unresolved questions regarding the crystallization of salts in confined environments [13,21–23]. In particular, the following issues remain inadequately understood or documented.

Role of non-confined face growth: it is not fully clear how growth on unconfined crystal faces competes with or limits the pressure exerted by a confined face. Experiments suggest that if a crystal can grow outward into an open space or if other crystals can nucleate and grow freely in the solution [22], the confined crystallization pressure may dissipate or never develop fully.

Effect of surface wettability on mass transport: a key factor enabling crystallization pressure in pores is the presence of a liquid nanolayer between the crystal face and the pore wall. By sustaining a thin solution layer at the interface, the repulsive disjoining pressure enables continued crystal growth against the confinement, whereas a crystal that directly bridges the pore (without a separating liquid film) cannot further grow or build up pressure [2]. The thickness and stability of this film must therefore depend on surface wetting properties.

Lifting mechanism: it is still unclear how lifting occurs on an atomic scale. What are the conditions for a crystal to increase its thickness when it is confined between two surfaces?

Considering the above knowledge gaps, the current study is designed with an emphasis on fundamental understanding. This work focuses on a model crystallization system and aims to obtain high quality, reproducible data under well-controlled conditions. The specific objectives of the study are to identify critical factors and limitations in crystallization pressure build-up. We systematically examine how the degree of solution supersaturation, the applied load (pressure), the interfacial energy (wettability), and the crystallographic orientation of the growing crystal faces affect crystallization pressure. To realize this we developed an experimental methodology that produces reproducible measurements of crystallization pressure, avoiding the large scatter often seen in past studies. We finally propose a mechanism for how lifting occurs.

2. Materials and methods

Single crystals of potassium aluminium sulphate dodecahydrate, commonly known as potash alum ($KAl(SO_4)_2 \cdot 12H_2O$, space group $Pa\bar{3}$) were selected for the experiments because of their rapid growth rate and the ability to prepare solutions with high supersaturation levels that are stable for a long time. For the same reasons, this material was used in many of the earlier experiments [7,9,10]. The growth rates of different crystal faces differ slightly ($G_{\{111\}} < G_{\{100\}}$) [24], which provides an opportunity to investigate how growth anisotropy influences the crystallization pressure. High-purity seed crystals of potash alum were grown from aqueous solution in the lab, using salt with a purity of 99.5 % (Sigma-Aldrich, 31242), with typical dimensions of 2×3×2 mm^3. Two sets of crystals were prepared and tested: one set had two parallel {111} faces, and the other set was cut to have parallel {100} faces. We found no significant difference between as-grown or cut {111} faces. By using preparation conditions that are as much the same as possible, we found good experimental reproducibility.

All experiments were performed at a temperature of 21.5±0.5 °C; the small temperature variation has no significant effect on the solubility at the levels of supersaturation used. The solubility at this temperature is known and thus a supersaturated solution can be made by dissolving an excess amount of potash alum at elevated temperature [25]. This solution is subsequently cooled down slowly to 21.5 °C, yielding a clear solution with the intended supersaturation. The relative supersaturation σ is defined as

$$\sigma = \frac{m - m_0}{m_0} \times 100\ \%, \tag{4}$$

where m is the molality of the prepared solution and m_0 is the molality of a saturated solution at 21.5 °C.

The confined crystal growth experiments were carried out using a single crystal with two opposite, parallel faces oriented horizontally under a mechanical load. The crystal was placed at the bottom of a flat cylindrical glass support which acted as the lower confining surface. A second glass cylinder (serving as a weight) was then gently placed on top of the crystal (Fig. 2). The top glass cylinder had a mass of 56 g for most experiments and exerts a force of approximately 0.5 N on the crystal (after subtracting the buoyant force due to its immersion in solution). The load of the potassium alum crystal itself is insignificant compared to this. The entire assembly (glass support, crystal, and top weight) was then filled with the supersaturated solution of known σ. To avoid trapping of air bubbles between the crystal and the glass surfaces, the apparatus was initially tilted at a slight angle as the solution was introduced, and then slowly brought to a level position (perpendicular to the table) once the crystal was fully submerged. For experiments with a different load, thinner glass cylinders were used or additional weights were added to the top glass cylinder.

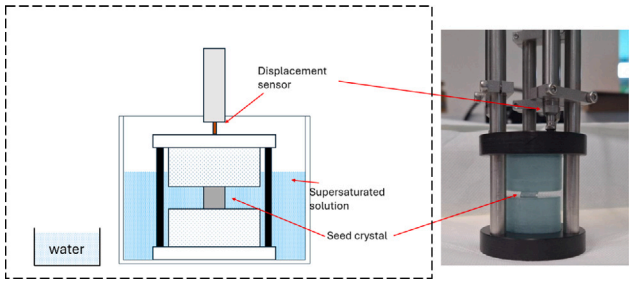

Fig. 2. Illustration of the experimental setup (side view): a single potash alum crystal is placed on a glass substrate at the bottom of a container and a glass cylinder weight rests on the top face of the crystal. In the right image two additional displacement sensors are visible which allow to monitor any tilt of the top glass cylinder.

At the start of each test, the crystal was completely immersed in the supersaturated solution, and the load was resting on the top face. The vertical displacement (height change) of the top glass weight was monitored over time using a Solartron incremental displacement sensor (Fig. 2). The sensor probe contacted the top of the weight and recorded any upward movement (crystal growth) or downward movement (crystal dissolution) with high sensitivity. Data were acquired continuously via a computer interface. The displacement sensor had an accuracy of 0.16 μm and a step of measurement of 0.125 μm, allowing to detect sub-micrometre changes in the crystal's height under load. The error in the measurement data was calculated as the sum of standard deviation and displacement sensor accuracy.

Throughout the experiments, the supersaturation gradually decreased as the crystal grew and consumed solute. To minimize evaporation of the solution (which could otherwise alter the supersaturation), the relative humidity in the chamber was maintained at RH ≈ 70±10 % by including a water reservoir near the sample. Towards the end of nearly all lifting experiments, after most of the lifting was completed, some secondary crystals formed in the set-up, which further reduced the supersaturation. In some of the experiments secondary crystals appeared already within the first two hours, causing a rapid decrease in the supersaturation. These experiments were therefore excluded.

The concentration of the potash alum solution was checked at the beginning and the end of each experiment to confirm the change in supersaturation. Small 50 μl droplets of solution were extracted from near the crystal and allowed to evaporate. The mass of the crystallized salt from each droplet was then measured using a high-precision balance (±0.001 mg). From this, the concentration of solute in the solution at those times could be determined, verifying the decrease in supersaturation over the course of the experiment and specifically the return to saturation when the experiment was continued until all growth (and lifting) was completed.

To ensure that the measured displacements represent the true height change of the crystal (and not artifacts of the setup), we performed a

number of tests without crystals and with or without solution, but with otherwise the same conditions. Because of temperature variations in the laboratory, we typically find a drift that stays within 1 μm over the time scales of our experiments and therefore height differences from growth or dissolution have to be larger than this value to be significant. In addition, in later experiments, two extra sensors were added on opposite sides of the top glass cylinder (Fig. 2) to monitor any tilting of the weight during the run. From the three-sensor readings, we can calculate and extract the true vertical component of the weight's movement, eliminating any influence of tilt. The significance of the results is finally determined by repeating most experiments several times.

At the end of each experiment, the crystal was immediately removed from the solution and immersed in acetone. This procedure rapidly displaces the aqueous solution and dries the crystal, thereby preventing any further uncontrolled crystallization or dissolution from residual solution on the crystal surfaces. After this step, the crystal was characterized to assess any changes in its mass, dimensions, and surface morphology. Detailed examination of the crystal surfaces was performed using optical microscopy and surface profilometry. Each face (top and bottom) was inspected under a light microscope to qualitatively identify features indicative of growth or dissolution (such as growth step patterns or etch pits). To quantify the surface topography, a stylus profilometer (Dektak XT) was used to measure height profiles across the crystal faces, with a vertical resolution of 20 nm. Line scans were taken along the centre of both the top and the bottom face after the experiment to determined the change in surface contour on each face and the relative height change.

In order to evaluate the results of the experiments, it is important to know the relation between pressure and supersaturation [14]. For potash alum this can be estimated in the following way. The dissolution of potash alum involves 16 ions/molecules:

$$KAl(SO_4)_2 \cdot 12H_2O \rightleftharpoons K^+ + Al^{3+} + 2SO_4^{2-} + 12H_2O. \tag{5}$$

The calculation is easiest when assuming ideal behaviour. Potash alum contains both ions and water (which is the solvent used) and these need to be treated differently. For the ions, the activity can be approximated by the product of molalities. For the saturated bulk solution we then obtain:

$$a_{0,\mathrm{ideal,ions}} = \left(m_{0,\mathrm{K}}\right)\left(m_{0,\mathrm{Al}}\right)\left(m_{0,\mathrm{SO_4}}\right)^2. \tag{6}$$

For the solution in (local) equilibrium with the loaded face, we get the same expression, but with '0' replaced by 'load'. The ratio of loaded and unloaded activities is for all ions the same, and the total ratio can be written as:

$$\frac{a_{\mathrm{load,ideal,ions}}}{a_{0,\mathrm{ideal,ions}}} = \left(\frac{m_{\mathrm{load}}}{m_0}\right)^4 = (1+\sigma)^4. \tag{7}$$

The ratio therefore only contains the supersaturation as (dimensionless) parameter.

For water, ideal behaviour means that the activity can be approximated by the mole fraction x_{W}. The calculation of the water activity in a (super)saturated solution of potash alum involves the actual values of the molalities. For potash alum, the solubility is 120 gr per 1 kg of water at 21.5 °C, corresponding to $m_0 = 0.254$ mol/kg. The molality of water is $m_{\mathrm{W}} = 55.5$ mol/kg. When a supersaturated solution is made, an amount $(1+\sigma)m_0$ potash alum is added to an amount m_{W} of water. The added potash alum contains 4 ions, but also 12 water molecules per mol, thus the total amount of water increases as well. This leads to the following expression for the mole fraction in a supersaturated solution:

$$x_{\mathrm{W}} = \frac{12(1+\sigma)m_0 + m_{\mathrm{W}}}{16(1+\sigma)m_0 + m_{\mathrm{W}}}. \tag{8}$$

For $\sigma = 0$ this equals the mole fraction $x_{0,\mathrm{W}}$ of a saturated solution.

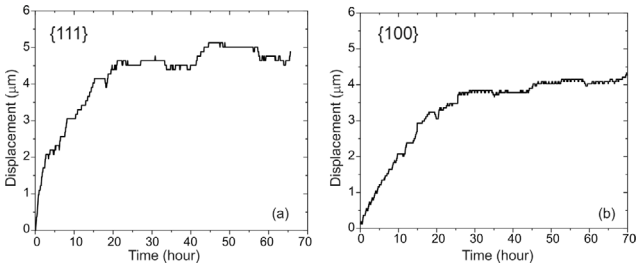

Fig. 3. Crystallization-induced displacement under load for a representative run for a crystal where the loaded surface has (a) a {111} and (b) a {100} orientation. In both cases a 0.5 N load in an initial 40 % supersaturated solution were used.

The ratio of activities of a supersaturated and a saturated solution, including both ions and water, then becomes:

$$\frac{a_{\mathrm{load,ideal}}}{a_{0,\mathrm{ideal}}} = \left(\frac{m_{\mathrm{load}}}{m_0}\right)^4 \left(\frac{x_{\mathrm{W}}}{x_{0,\mathrm{W}}}\right)^{12}. \tag{9}$$

Substituting this in Eq. (1), we obtain for the crystallization pressure:

$$\Pi_{\mathrm{ideal}} = \frac{RT}{V_m}\left[4\ln\left(\frac{m_{\mathrm{load}}}{m_0}\right) + 12\ln\left(\frac{x_{\mathrm{W}}}{x_{0,\mathrm{W}}}\right)\right]. \tag{10}$$

This can be written as a function of the supersaturation σ as:

$$\Pi_{\mathrm{ideal}} = \frac{RT}{V_m}\left[4\ln(1+\sigma) + 12\ln\left(\frac{1+\frac{12m_0}{12m_0+m_{\mathrm{W}}}\sigma}{1+\frac{16m_0}{16m_0+m_{\mathrm{W}}}\sigma}\right)\right]. \tag{11}$$

For potash alum, $V_m = 2.75\times10^{-4}$ m^3. Substituting the values of m_0, m_{W} and the temperature of 21.5 °C (294.5 K), gives:

$$\Pi_{\mathrm{ideal}} = 8.9\left[4\ln(1+\sigma) + 12\ln\left(\frac{1+0.052\sigma}{1+0.068\sigma}\right)\right] \text{ MPa}. \tag{12}$$

For $\sigma = 0.3\,(30\ \%)$, we find a crystallization pressure of approximately 8.8 MPa or 88 bar. Flatt et al. [13] show in their Fig. 2 not only this ideal result, but also that for a calculation using activities (thus not assuming ideal behaviour) and find a pressure that is about half this value. While we do not require a high accuracy for the purpose of this paper, we will apply this correction and use:

$$\Pi \simeq 0.5\,\Pi_{\mathrm{ideal}}. \tag{13}$$

We therefore estimate that $\sigma = 0.3$ corresponds to 4.4 MPa.

3. Results

3.1. Crystallization-induced lift under load

In a typical experiment ($\sigma = 40$ % initial supersaturation, {111} crystal orientation, normal glass), the vertical displacement of the crystal was observed to increase slowly over time under the 0.5 N load, see Fig. 3a. The crystal's height increased continuously, with a final gain of 5.0 ± 0.3 μm after 70 h. The upward displacement of the load directly confirms that the crystal growth generates force against the weight. The time evolution of the displacement is not linear: it consists of an initial rapid-growth phase, followed by a plateau by the end of the experiment. This shows that the crystal grew quickly at first (when the supersaturation was highest) and then the growth rate gradually decreased as the local supersaturation was consumed and approached saturation ($\sigma = 0$ %).

Profilometry of the crystal surfaces after the experiment provides insight into the location of the newly grown salt. Fig. 4 illustrates the surface height profile of the crystal's top and bottom faces after 14 h. It is evident that newly grown material did not uniformly coat the side face to meet the upper glass, but instead formed a rim at the bottom interface instead. The crystal thus grew primarily at its bottom edge,

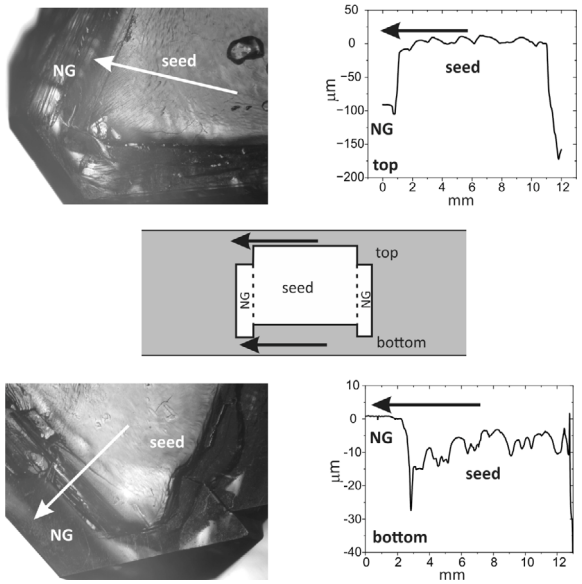

Fig. 4. Optical microscopy images and surface profilometry results of a crystal after 14 h growth, showing the height profiles of the top face and bottom face. The arrows indicate the trace of the profilometer. NG indicates new growth parts of the crystal.

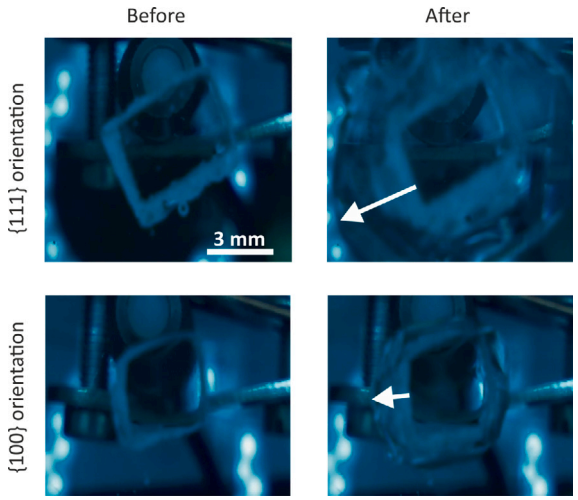

Fig. 5. In situ photographs at the start and after 10 h of growth. Crystals are viewed from the bottom glass cylinder and show side growth as indicated by the arrows (σ = 40 % initial supersaturation 0.5 N load). The {111}-oriented crystal shows more side growth than the {100}-oriented crystal, in agreement with the difference in growth rates of the side faces. All images are on the same scale.

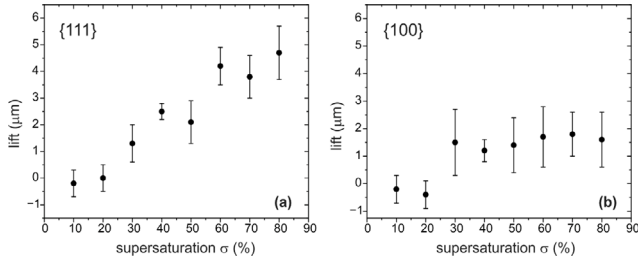

Fig. 6. Vertical displacement (Δh) *vs.* initial supersaturation for both orientations with 0.5 N load, demonstrating that {111} crystals (a) achieve higher lifts than {100} (b) at high supersaturation.

effectively pushing itself and the attached weight upward. The top face (directly beneath the weight) remained largely unchanged and flat. The difference between top and bottom arises from the difference in supersaturation: once growth commences, convection over the 2–3 mm thickness of the crystal leads to a lower supersaturation at the top. This behaviour has been observed before [8,9,21].

We performed similar experiments for loaded surfaces with a {100} orientation. As shown in Fig. 3b, also here the crystal's height increased continuously, but with a smaller final height gain of 4.0 ± 0.3 μm after 70 h.

Along with the vertical growth (which causes lifting of the weight), significant side face growth is observed in these experiments for both orientations, see Fig. 5. As the seed crystal grows, it extends its footprint outward along the substrate surface, forming a rim as already shown in Fig. 4. We find that crystals with {111} faces as the top and bottom show more extensive side growth. This leads to a larger lift compared to {100}-oriented crystals. These observations highlight that crystallographic orientation can affect the amount of lifting.

3.2. Lifting threshold and dependence on supersaturation

A series of experiments was conducted to examine how the vertical lifting Δh produced by the crystal depends on the solution supersaturation. The vertical displacement of the top glass weight (0.5 N) after a fixed duration (16–18 h) was measured for supersaturation levels ranging from 10 % up to 80 %; both {111} and {100} oriented crystals were tested. The results, summarized in Table 1 and plotted in Fig. 6, show a clear dependence of lifting on supersaturation. No measurable lifting is observed for supersaturations at the low end of the range (σ = 10–20 %); in these cases the recorded Δh is close to zero or even slightly negative (suggesting a tiny amount of dissolution). This indicates that at these mild supersaturations the crystallization pressure is insufficient to overcome even the modest weight in our setup. A clear threshold behaviour is observed: once σ exceeds about 30 %, crystal growth generates enough force to produce an upward movement of the weight. For the {111} orientation the magnitude of lifting increases linearly with supersaturation above this threshold. For the {100} orientation the lift appears quite constant, even though

Table 1
Vertical displacement (Δh) of confined potash alum crystals under a 0.5 N load, for various solution supersaturation levels. Results are shown for two crystal orientations: {111} and {100} loaded faces. Values represent the mean Δh. The error is based on multiple experiments (excluding runs with early secondary nucleation). Negative values indicate a slight dissolution under load.

σ (%)	Δh (μm) {111}	# expt. {111}	Δh (μm) {100}	# expt. {100}
10	-0.2 ± 0.5	5	-0.2 ± 0.5	5
20	0.0 ± 0.5	5	-0.4 ± 0.5	5
30	1.3 ± 0.7	6	1.5 ± 1.2	7
40	2.5 ± 0.3	14	1.2 ± 0.4	8
50	2.1 ± 0.8	6	1.4 ± 1.0	6
60	4.2 ± 0.7	5	1.7 ± 1.1	5
70	3.8 ± 0.8	5	1.8 ± 0.8	5
80	4.7 ± 1.0	5	1.6 ± 1.0	5

the error bars are compatible with a small slope. This behaviour is probably caused by the fact that the slower side growth for the {100} case leads to a stronger depletion of the supersaturation in the system due to the formation of secondary crystals. For both the {111} and {100} orientations, once the available supersaturation was consumed by crystallization, the growth stopped.

Comparing the two orientations {111} and {100}, our findings appear to be counter-intuitive: the {100} is the faster-growing face, but produces less lift than the slower-growing {111} face. The explanation lies in the fact that, as already discussed above, the lift in the {100}

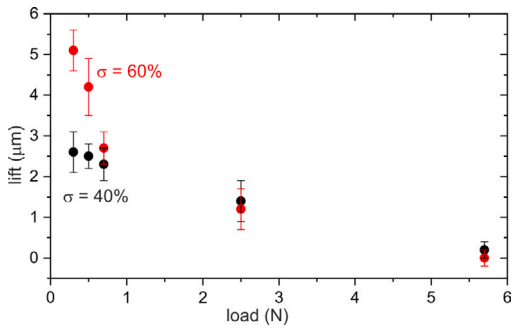

Fig. 7. The lift as a function of applied load on the {111} orientation for two values of the supersaturation.

Table 2
Vertical displacement Δh of confined potash alum crystals with {111} crystal orientations for various load levels. Results are shown for two initial supersaturation levels: $\sigma = 40$ and 60 %.

Applied load (N)	Δh (μm) $\sigma = 40$ %	# expt. $\sigma = 40$ %	Δh (μm) $\sigma = 60$ %	# expt. $\sigma = 60$ %
0.3	2.6 ± 0.5	4	5.1 ± 0.5	4
0.5	2.5 ± 0.3	14	4.2 ± 0.7	5
0.7	2.3 ± 0.4	4	2.7 ± 0.4	4
2.6	1.4 ± 0.5	3	1.2 ± 0.5	3
5.7	0.2 ± 0.2	3	0.0 ± 0.2	3

direction involves side face growth in the slower {111} direction, and vice versa. We will come back to this in the discussion section.

3.3. Effect of applied load

Although supersaturation provides the thermodynamic driving force for crystallization, the mechanical load (external pressure) limits how much of that can be used for lifting. We therefore performed a series of experiments with different applied loads. The results show that the heavier the applied load, the smaller the maximum Δh, see Fig. 7 and Table 2. Under the highest tested load (5.7 N), no lifting is observed for both a σ of 40 % or 60 %. This means that there exists an upper limit to the crystallization pressure that a given supersaturated solution can support; once the external pressure exceeds that limit, the crystal will only grow sideways.

The theory predicts that in the absence of supersaturation, the crystal should dissolve when loaded. The stress in the loaded crystal face raises its chemical potential such that the solution in the nanolayer reaches a higher saturation level than the bulk solution. Mass transport from the nanolayer to the bulk solution subsequently lowers the concentration in the nanolayer, resulting in dissolution. To validate this prediction, we exposed a crystal that had previously lifted a weight under high supersaturation, to a saturated solution ($\sigma = 0$ %), while still under external pressure. The results in Fig. 8 show a pronounced dissolution that increases when a higher load is applied. Unlike the growth experiments, dissolution does not level off, because in this case the driving force (i.e. the difference in concentration between nanolayer and bulk) remains constant.

After the dissolution, we examined the crystal surfaces. Fig. 9 shows an optical micrograph of a crystal after it had dissolved for 20 h, with clear signs of dissolution damage: etch pits formed on the crystal surface, and the edges and corners of the crystal have become more rounded compared to their sharp form observed after growth. Interestingly, the dissolution is not uniform across the surface. The centre of the crystal's face shows fewer dissolving signs than the edges. This uneven pattern can be explained by dissolution kinetics in the confined setup. The geometry limits mass transport from the central region compared to that from the edges.

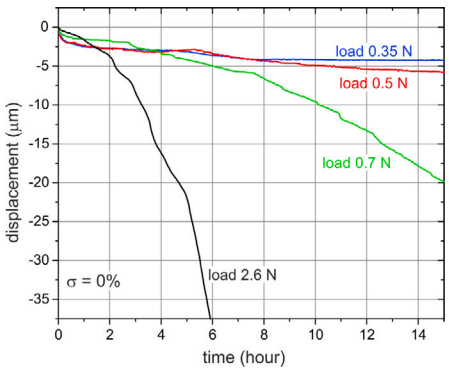

Fig. 8. Vertical displacement of the crystal *vs* time when a previously grown crystal under load is placed in a saturated solution ($\sigma = 0$ %). This demonstrates that the crystallization pressure effect is reversed when supersaturation is removed.

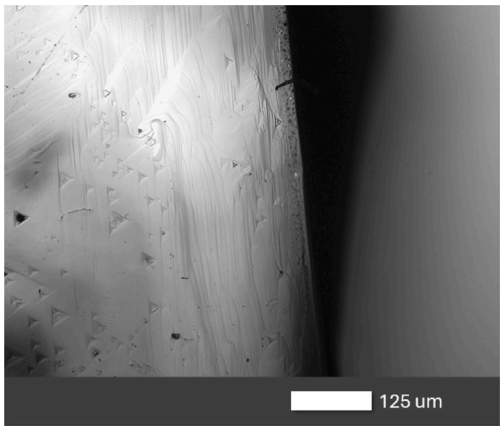

Fig. 9. Optical micrograph of a crystal surface after 20 h of dissolution under load. Numerous etch pits are visible on the surface (triangular features) as well as rounded-off and eroded crystal edges.

Once the supersaturation in the bulk is raised to the threshold level corresponding to the applied load, dissolution should stop and that is confirmed by the experimental results presented in Fig. 10. Here, after a period of dissolution at $\sigma = 0$ %, the supersaturation is raised to $\sigma = 20$ %, $\sigma = 30$ % or 40 % in Figs. 10(a), (b) and (c), respectively. It is important to note that there is a difference between the threshold supersaturation for dissolution and that needed for lifting the weight. In fact, a supersaturation of 20 % is enough to stop dissolution, but not enough to start lifting of the weight. Fig. 11 displays optical microscopy images of the crystal surface that had undergone the change in σ from 0 % to 30 %, revealing characteristic features of both growth and partial dissolution.

3.4. Effects of surface wettability

The supply of solution to or from the confined growth interface and thus the presence of liquid film (the nanolayer) is a crucial factor controlling crystallization when a pressure is applied. The existence and thickness of the nanolayer depends on the interfacial energies and thus on the wettability of the surfaces. To investigate the role of substrate wettability in confined crystallization, we compared the results on lifting found so far obtained on normal glass (which is slightly hydrophilic) with crystals growing on a hydrophilic surface (mica) and a hydrophobic surface (silanized glass). Table 3 summarizes the results for both the {111} and {100} orientation. The hydrophilic mica yields

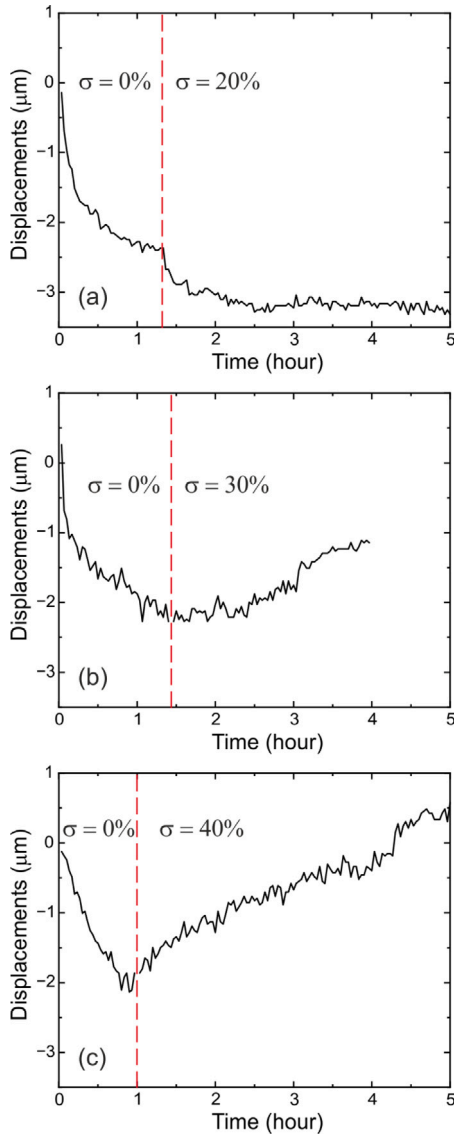

Fig. 10. Displacement–time curves starting with a dissolution period with σ = 0 % and, at the time indicated by the red, dashed line, a subsequent increase of the supersaturation to (a) 20 %, (b) 30 % or (c) 40 %. The load is 0.5 N for all cases. (For interpretation of the references to colour in this figure legend, the reader is referred to the web version of this article.)

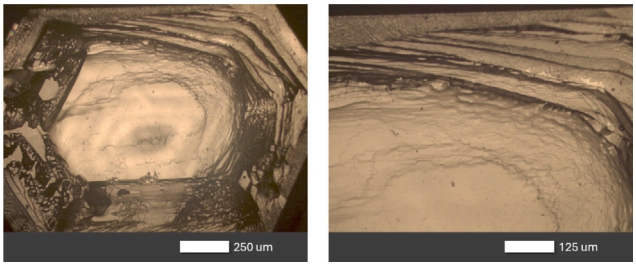

Fig. 11. Optical microscopy images at two magnifications of the crystal used for Fig. 10b after the σ = 0 % to 30 % supersaturation change.

Table 3
Vertical displacement (Δh) of confined potash alum crystals under a 0.5 N load and σ = 40 % supersaturation, for various surface hydrophilicities. Results are shown for two loaded crystal orientations: {111} and {100}. The values represent the mean Δh after 16 h of growth. The error bar is based on averaging multiple experiments (excluding runs with early secondary nucleation).

Hydrophilicity	Δh (μm) {111}	# expt. {111}	Δh (μm) {100}	# expt. {100}
++ mica	3.2 ± 0.9	5	2.2 ± 0.7	4
+ normal glass	2.5 ± 0.3	14	1.2 ± 0.4	8
– silanized glass	0.5 ± 0.3	4	0.3 ± 0.3	4

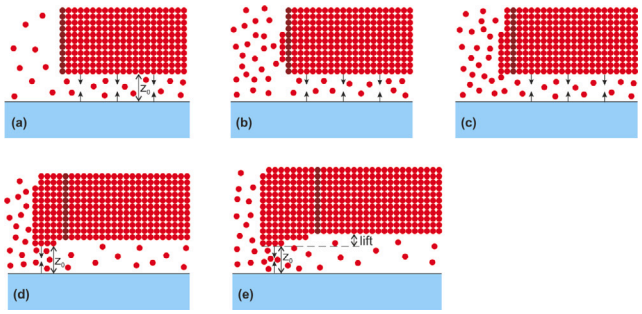

Fig. 12. Schematic representation of the proposed mechanism leading to the observed lift of the crystal via disjoining pressure. The crystal is assumed to carry a significant weight (not shown), leading to a pressure at the bottom interface. To see the new growth area more clearly, the atoms of the initial edge of the crystal have been given a darker colour. (For interpretation of the references to colour in this figure legend, the reader is referred to the web version of this article.)

a somewhat larger lift than normal glass, while no significant lift is observed on the hydrophobic glass.

The presence or absence of the liquid nanolayer should also affect the dissolution in a saturated solution. In the case of normal, hydrophilic glass as substrate, Fig. 8 showed the significant dissolution. We performed a number of tests using hydrophobic glass instead, pressing again cut {111} faces. As expected, we did not see dissolution in this case, even under a load of 2.6 N. The absence of the liquid nanolayer when using a hydrophobic substrate means that mass transport from the interface area is too limited to lead to significant dissolution. To check that the lack of dissolution in this case was not caused by a difference in the interface geometry, we used the same crystals also in combination with normal (hydrophilic) glass. Here a high load again resulted in dissolution.

4. Discussion

To arrive at a proposed lifting mechanism, we first summarize the main experimental results. We have found that lifting only occurs above a threshold supersaturation value as long as the load is not too high. Lifting involves side growth that generates a rim around the starting crystal and more side growth leads to more lifting. When the bulk solution is saturated, a sufficiently large load leads to dissolution. And finally, no lifting occurs when the confining surface is hydrophobic. These observations are consistent with classical concepts of crystallization pressure as formulated by Correns and extended by Steiger and others [2,5,13,14,18,22].

Together, these observations bring us to an atomic-scale model for the mechanism behind the occurrence and size of lift, and with that of the crystallization pressure. This is illustrated in Fig. 12. An essential ingredient in generating lift, is the presence of a nanolayer between crystal and support, see Fig. 12a. There must be a repulsive disjoining force, which requires interfacial energies that favour a gap. In aqueous

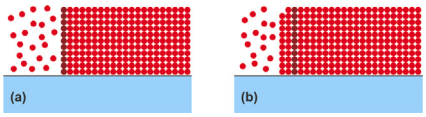

Fig. 13. A schematic of the situation when the load is so high that the nanolayer disappears. No lifting occurs and the only growth on the side faces takes place.

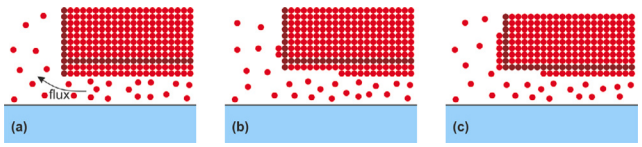

Fig. 14. Schematic of dissolution in a saturated solution. The nanolayer solution has a higher concentration and mass is transported to the bulk solution, leading to dissolution at the bottom of the crystal. The small increase in supersaturation in the bulk leads to moderate side growth. To show the mechanism more clearly, a horizontal row and a vertical column of atoms have been given a darker colour. (For interpretation of the references to colour in this figure legend, the reader is referred to the web version of this article.)

solutions, this means that the solids must be hydrophilic. In addition, the load on the crystal should not generate a pressure higher than the maximum disjoining pressure. Fig. 12a shows an idealized surface, where the disjoining force is evenly distributed over the full area, but in reality there will be thickness variations in the nanolayer and the pressure will be highest at the location of the thinnest layer. Fig. 12a represents a situation in which the bulk solution is saturated, thus no growth occurs at the unloaded face and no lifting is possible. Due to the pressure, the solution concentration in the nanolayer is higher than in the bulk solution.

Fig. 12b shows the initial stage of lifting when a sufficiently large supersaturation (above the threshold) is present in the bulk solution. This first of all leads to growth on the unloaded side faces. Simultaneously, it should in principle allow growth within the gap and thus lift the weight, but mass transport through the nanolayer is limited and this process is insignificant. However, at the rim of the crystal, mass transport is not a limitation and atoms will occasionally attach to a location within the gap and growth occurs (see Fig. 12c). This corresponds to a locally increased disjoining force and the atom will only survive if the local concentration is high enough. From the observed ratio of lateral growth (several millimetres) and lift (several micrometres), the growth probability within the nanolayer is about a factor one thousand smaller than on the side face. The growth will continue (Fig. 12d) and at some point a small rim is formed able to exert enough force to take over the disjoining force from the initial bottom crystal surface. The local concentration at the initial surface will thus decrease, eventually reaching the bulk saturation value. The process described here will repeat itself, and a new rim will form, lifting the entire crystal once more (Fig. 12e). In this way a crystal with a hollow bottom is formed. The model shows that lifting is only possible when side growth occurs. The figure gives a two-dimensional view: in reality, when locally a new crystal layer in the nanolayer is formed, it will spread laterally across the rim, which is a process that is energetically and kinetically relatively easy. Note that crystals with a hollow bottom are also frequently observed when crystals are formed at the bottom of a vessel in solution growth. In that case the crystal itself provides the load on the bottom interface, thus without the presence of an additional weight.

The thickness of the nanolayer is determined by the balance of the disjoining force and the applied load [17]. The disjoining force depends strongly on the distance between the interfaces, and a smaller load will give a somewhat larger distance. Similarly, a more hydrophilic interface will also give a larger distance. A thicker nanolayer facilitates lift, because it is easier to attach growth units below the existing surface; this agrees with our observations.

As stated above, lifting requires the presence of a nanolayer. If the load is so high that it generates a pressure that is larger than the maximum disjoining pressure, the nanolayer will collapse and the load is supported by the force across the solid–solid interface of crystal and support. The nanolayer will also collapse (or not form) if the interfacial energies make this more favourable, as in the case of the experiments with a hydrophobic glass. Fig. 13 sketches the evolution of the system in case no gap (and nanolayer) is present: there is no opportunity for atoms to attach below the crystal surface and only side growth occurs. Fig. 13 sketches an idealized situation; in reality the solid interfaces are not perfectly flat and the solution will only be removed at the locations where the solids actually touch. At other locations (like hollow parts at the bottom of the crystal), there will still be a solution layer present, but this will not have sufficient supersaturation to lead to growth, let alone lifting.

Without bulk supersaturation, a load will lead to dissolution of the crystal. Fig. 14 shows this in more detail. The load causes the local equilibrium in the nanolayer to correspond to a higher concentration than in the bulk saturated solution; this leads to a mass flow from the nanolayer to the bulk solution. This will result in side growth and a thinning of the crystal. The extent of this depends on the details of the geometry, but this effect will be limited when the load, and thus the concentration difference, is small. This is why we observe only significant dissolution when the load is high enough.

The literature shows that it is nearly impossible to quantitatively compare the relation between lifting and supersaturation [13]. Here we will therefore only do a rough evaluation. The first estimate is from the observed lift for a constant load. We find from the data shown in Fig. 6 (and confirmed by the data in Fig. 11) a threshold supersaturation of 25 ± 5 % for a load of 0.5 N. The total bottom surface area of the crystal varies from crystal to crystal and changes during growth, but we can use a typical value of 8×10^{-6} m^2. If the load was evenly distributed, this would correspond to a pressure of 63 kPa. Using Eqs. (12) and (13), the crystallization pressure for the experimental threshold supersaturation is 3.8 ± 0.6 MPa, which is a factor 60 higher. This large discrepancy can be explained by the fact that only a small fraction of the surface of the growing crystal contributes to the lifting. The factor 60 difference means that only about 1.5 % of the surface area participates in the lifting. While it is difficult to accurately estimate the area contributing to the lifting, the experiments show that only a narrow rim of the growing crystal is in contact with the bottom surface; a contact area of a few % as calculated above is therefore very reasonable.

A second estimate is from the measured lift as a function of applied load, shown in Fig. 7. For both σ = 40 and 60 %, we find lift at a load of 2.6 N and no lift at 5.7 N. We can summarize this as a threshold supersaturation of 50 ± 10 % at a load of 4.1±1.6 N. This load corresponds to an average pressure of 0.5 ± 0.2 MPa, while the supersaturation corresponds to a crystallization pressure of 6.8 ± 0.6 MPa. This implies a contact area of 7 ± 3 % of the total surface area. This is a much larger than the first estimate, but still a small fraction of the total surface. Similar conclusions were reached by Desarnaud et al. [5] and by other micro-scale studies, where true contact areas were as small as 0.1 % of the total face, leading to pressures larger than 100 MPa during NaCl growth [5].

We thus find that lifting only occurs when three conditions are fulfilled

1. A liquid nanolayer is present. This requires specific interfacial properties such that the solution wets the interface and there is a large enough disjoining pressure across the nanolayer. This finding aligns with long-standing theories that crystallization pressure requires a wetting film at the contact interface [2,22,26].

2. Growth at the side faces occurs. Because mass transport within the nanolayer is too limited, growth within the nanolayer is only possible at the rim of the crystal and this is enabled by growth at the side faces.
3. Threshold supersaturation. The lower face of the crystal is under pressure, corresponding to a higher solution concentration in order to have local equilibrium. This is a higher supersaturation with respect to the unloaded side face. Growth at the bottom face can thus only occur if the supersaturation exceeds that of the local equilibrium concentration.

Considering the conditions listed above, there are three options for preventing lifting and the corresponding crystallization damage.

1. Prevent the presence of a nanolayer by modifying the surface energies of the interfaces involved. This corresponds to reducing the wettability of the interfaces.
2. Prevent side growth. This can be done by growth inhibitors, and is the likely mechanism for the reduced damage from NaCl crystallization when the growth inhibitor ferrocyanide is applied [27–30].
3. Reduce the supersaturation. This can be done by inducing the growth of many crystals, e.g. by using a nucleation agent or having surfaces present that stimulate heterogeneous nucleation. This effect also plays a role in the NaCl-ferrocyanide combination mentioned above [27].

Finally, we would like to mention that the relation between pressure and solution activity (concentration) has been derived by considering the equilibrium of a stressed surface with a bulk solution [14]. The solution in the nanolayer, however, is expected to have different properties than such a bulk solution, because it will exhibit considerable layering induced by the immediate vicinity of solid surfaces. This will modify the ion/molecule activities compared to a bulk solution, but qualitatively the effects we described remain the same. Quantifying the relation between pressure and supersaturation is thus a challenge that remains to be overcome both experimentally and theoretically. Recent computer simulations have started to address this issue [17].

5. Conclusion

This study demonstrates a reproducible method to measure crystallization pressure via the lifting caused by salt crystal growth in a confined set-up. Crystal growth from sufficiently high supersaturation can generate measurable forces that cause vertical displacement of an overlying load. The magnitude of this displacement depends on both the driving force (supersaturation level) and the boundary conditions (mechanical load and surface wettability). Hydrophobic (non-wetting) surfaces and heavy loads tend to limit the lifting by, respectively, restricting mass transport and requiring higher supersaturation for growth. In contrast, lighter loads and hydrophilic conditions allow the crystal to fully develop its crystallization pressure, leading to greater lifting.

These findings contribute to a deeper understanding of damage mechanisms in porous materials due to salt crystallization and can inform strategies for salt damage mitigation. Our observations are consistent with fundamental crystallization pressure concepts and with prior studies in the literature, lending confidence that this model experiment captures the essence of salt weathering phenomena. In bridging classic qualitative demonstrations [7] with modern analyses, the study underscores the importance of both chemistry (supersaturation) and physics (confinement and mechanics) in salt-induced deterioration of materials.

CRediT authorship contribution statement

Anton Tuluk: Writing – original draft, Visualization, Validation, Methodology, Investigation, Formal analysis, Conceptualization. **Erik de Ronde:** Methodology, Investigation. **Michael Steiger:** Writing – review & editing. **Barbara Lubelli:** Writing – review & editing, Funding acquisition. **Hugo Meekes:** Writing – review & editing, Supervision, Conceptualization. **Elias Vlieg:** Writing – review & editing, Visualization, Supervision, Formal analysis, Conceptualization.

Declaration of competing interest

The authors declare that they have no known competing financial interests or personal relationships that could have appeared to influence the work reported in this paper.

Data availability

Data will be made available on request.

References

[1] A. Goudi, H. Viles, Salt Weathering Hazards, Wiley & Sons, 1997.
[2] A.E. Charola, Salts in the deterioration of porous materials: An overview, J. Am. Inst. Conserv. 39 (2000) 327–343, http://dx.doi.org/10.1179/019713600806113176.
[3] E. Doehne, Salt weathering: A selective review, Geol. Soc. Spec. Publ. 205 (2001) 51–64, http://dx.doi.org/10.1144/GSL.SP.2002.205.01.05.
[4] R. Flatt, F. Caruso, A. Sanchez, G. Scherer, Chemomechanics of salt damage in stone, Nat. Comm. 5 (2014) http://dx.doi.org/10.1038/ncomms5823.
[5] J. Desarnaud, D. Bonn, N. Shahidzadeh, The pressure induced by salt crystallization in confinement, Sci. Rep. 6 (2016) 30856, http://dx.doi.org/10.1038/srep30856.
[6] R. Flatt, A. Nevin, F. Caruso, H. Derluyn, J. Desarnaud, B. Lubelli, R. Espinosa-Marzal, L. Pel, C. Rodriguez-Navarro, G. Scherer, N. Shahidzadeh, M. Steiger, Predicting salt damage in practice: a theoretical insight into laboratory tests, RILEM Tech. Lett. 2 (2017) 108–118, http://dx.doi.org/10.21809/rilemtechlett.2017.41.
[7] G.F. Becker, A.L. Day, The linear force of growing crystals, Proc. Wash. Acad. Sci. VII (1905) 283–288.
[8] G.F. Becker, A.L. Day, Note on the linear force of growing crystals, J. Geol. 24 (1916) 313–333.
[9] S. Taber, The growth of crystals under external pressure, Am. J. Sci. 41 (1916) 532–556.
[10] C.W. Correns, W. Steinborn, Growth and dissolution of crystals under linear pressure, Z. Krist. A 101 (1939) 117.
[11] C.W. Correns, Growth and dissolution of crystals under linear pressure, Disc. Faraday Soc. 5 (1949) 267.
[12] G.W. Scherer, Crystallization in pores, Cem. Concr. Res. 29 (1999) 1347–1358, http://dx.doi.org/10.1016/s0008-8846(99)00002-2.
[13] R.J. Flatt, M. Steiger, G.W. Scherer, A commented translation of the paper by C.W. Correns and W. Steinborn on crystallization pressure, Env. Geol. 52 (2007) 187–203, http://dx.doi.org/10.1007/s00254-006-0509-5.
[14] M. Steiger, Crystal growth in porous materials-I: The crystallization pressure of large crystals, J. Cryst. Growth 282 (2005) 455–469, http://dx.doi.org/10.1016/j.jcrysgro.2005.05.007.
[15] J. Desarnaud, O. Grauby, P. Bromblet, J. Vallet, A. Baronnett, Growth and dissolution of crystal under load: New experimental results on KCl, Cryst. Growth Des. 13 (2013) 1067–1074, http://dx.doi.org/10.1021/cg3013359.
[16] F. Kohler, O. Pierre-Louis, D. Dysthe, Crystal growth in confinement, Nat. Comm. 13 (2022) http://dx.doi.org/10.1038/s41467-022-34330-5.
[17] B. Mahmoud Hawchar, T. Honorio, M. Vandamme, F. Osselin, J. Pereira, L. Mercury, L. Brochard, Exploring crystallization pressure limits via molecular simulation, J. Chem. Phys. 163 (2025) http://dx.doi.org/10.1063/5.0282117.
[18] M. Steiger, Crystal growth in porous materials-II: Influence of crystal size on the crystallization pressure, J. Cryst. Growth 282 (2005) 470–481, http://dx.doi.org/10.1016/j.jcrysgro.2005.05.008.
[19] B.V. Derjaguin, N.V. Churaev, V.M. Muller, Disjoining pressure, in: Surface Forces, Springer, MA, 1987, pp. 25–52, http://dx.doi.org/10.1007/978-1-4757-6639-4_2.
[20] J. Israelachvili, G. Adams, Measurement of forces between 2 mica surfaces in aqueous-electrolyte solutions in range 0-100 NM, J. Chem. Soc. Faraday Trans. 74 (1978) 975–1001, http://dx.doi.org/10.1039/f19787400975.

[21] A. Røyne, D.K. Dysthe, Rim formation on crystal faces growing in confinement, J. Cryst. Growth 24 (2012) 89–100, http://dx.doi.org/10.1016/j.jcrysgro.2012.03.019.
[22] P.K. Weyl, Pressure solution and the force of crystallization: a phenomenological theory, J. Phys. D 64 (1959) 2001–2025, http://dx.doi.org/10.1029/jz064i011p02001.
[23] E.P. Rothrock, On the force of crystallization of calcite, J. Geol. 33 (1925) 80–83.
[24] G. Botsaris, E. Denk, Growth rates of aluminum potassium sulfate crystals in aqueous solutions, Ind. Engin. Chem. Fund. 9 (1970) 276–283, http://dx.doi.org/10.1021/i160034a014.
[25] D. Schlain, J. Prater, S. Ravitz, Solubilities of ammonium and potassium alums in water - densities of the saturated solutions, Ind. Engin. Chem. 39 (1947) 74–76, http://dx.doi.org/10.1021/ie50445a026.
[26] L. Li, F. Kohler, A. Røyne, D. Dysthe, Growth of calcite in confinement, Crystals 7 (2017) 361, http://dx.doi.org/10.3390/cryst7120361.
[27] B. Lubelli, R. van Hees, H. Huinink, C. Groot, Irreversible dilation of NaCl contaminated lime-cement mortar due to crystallization cycles, Cem. Concr. Res. 36 (4) (2006) 678–687, http://dx.doi.org/10.1016/j.cemconres.2005.10.008.
[28] A. Bode, S. Jiang, J.M. Meijer, W.P. van Enckevort, E. Vlieg, Growth inhibition of sodium chloride crystals by anticaking agents: In situ observation of step pinning, Cryst. Growth Des. 12 (2012) 5889–5896, http://dx.doi.org/10.1021/cg3012537.
[29] S. Granneman, B. Lubelli, R. van Hees, Effect of mixed in crystallization modifiers on the resistance of lime mortar against NaCl and Na_2SO_4 crystallization, Constr. Build. Mat. 194 (2019) 62–70, http://dx.doi.org/10.1016/j.conbuildmat.2018.11.006.
[30] A. Kamat, E. Schlangen, B. Lubelli, Encapsulated crystallisation inhibitor as a long-term solution to mitigate salt damage in hydraulic mortars, Cem. Concr. Comp. 152 (2024) http://dx.doi.org/10.1016/j.cemconcomp.2024.105682.